Luminosity Spectrum and Top Quark Threshold Studies at the ILC

Filimon Gournaris

Supervisors:
Prof. D.J. Miller
Dr. S.T. Boogert

Department of Physics and Astronomy
University College London

March 23, 2005

Contents

Abstract

The luminosity spectrum is an important parameter of an accelerator, and thus must be understood and modeled precisely. In this study the different energy loss components of the luminosity spectrum are investigated, and improved methods for modeling them are devised.

Furthermore, a study of how the luminosity spectrum influences the top quark threshold is performed, by introducing uncertainties in our knowledge of the luminosity spectrum, and simulating the effects that such uncertainties would have on the top quark measurement.

It is found that uncertainties introduced in the beamstrahlung component of the luminosity spectrum by using the Bhabha acolinearity method for measuring it, do not influence the top quark measurement. By introducing random uncertainties for studying the effects in the beamspread and beamstrahlung components separately, the way that these uncertainties influence the top quark measurement is determined.

Finally, the percentage of the luminosity spectrum being effective for top quark production at the top threshold is determined by truncating the spectrum and examining the effects introduced to the top measurement.

1 Introduction

Physics in general relies upon the cross examination of theoretical and experimental results in order to understand nature. Particle physics is no exception to this rule, and thus theoretical results must be compared with their experimental counterpart, and vise versa, in order for progress to be made.

The current theoretical understanding of nature in its most fundamental form, the elementary particles and the forces between them, is provided by the so called Standard Model (SM) of particle physics. The SM has been heavily examined in experiments during the last 30 years, and no major disagreement between theory and experiment has been found. However, there are some important parameters of the model that still need to be examined in order to understand if nature behaves as described by the SM, or if there are other aspects and extensions that need to be added (eg SuperSymmetry).

The most important, and most famous, of these parameters is the Higgs boson, which in the model explains how particles acquire mass. The Large Hadron Collider (LHC) currently built at CERN is expected to find the Higgs boson, if such exists, and examine some of its properties. A second very important parameter of the SM that needs further examination are the properties of nature's heaviest fundamental particle, the top quark.

So far, since the discovery of the top quark in 1995, experimenters have managed to measure its mass to $M_t = 174.3 \pm 5.1$ GeV [1]. Because the top quark is so heavy (second heaviest, excluding the Higgs boson, is the the bottom quark with mass $M_b \approx 4.3$ GeV), it is very difficult to produce it in accelerators since a very large centre of mass energy is required. Most of our knowledge of the top quark comes from direct observations at the CDF and D0 experiments at Fermilab, and it is expected that when the LHC becomes operational in 2007, it will deliver a top quark mass measurement with uncertainty in the range of 1-2 GeV.

However, both the Tevatron and the expected LHC are hadron colliders, which do not provide the best environment to do precision physics. Therefore, just like after the SPS and ISR projects at CERN (both hadron colliders) an e^+e^- machine, LEP, was constructed, in order to do the precision physics of the discoveries of the W and the Z. In the same way, precision physics needs an e^+e^- collider to study the discoveries produced in the energy ranges of the LHC and the Tevatron. This machine will be an e^+e^- Linear Collider with energies of 0.5 to 1 TeV.

1.1 The ILC

Linear colliders offer the ideal environment to do precision physics, because the particles that they collide are themselves elementary (e^+ and e^-), and thus a very low background exists, while hadron machines collide protons, which are composed of quarks in a bath of gluons, where the background is very high.

The case for building a Linear Collider in the energy range of 0.5 to 1 TeV is being made since the early nineties, with different design proposals from the US-Japan and Europe. The US-Japan proposals focused on an accelerator with copper accelerating

cavities operating at room temperatures, while the European proposal (TESLA) [2] focused on a accelerator with superconducting cavities operating at 2 K. By the end of 2004, the decision was made to use the superconducting 'cold' approach, and thus all worldwide effort on the design of the machine is now concentrating on this approach, now called the International Linear Collider (ILC). Luckily, the machine assumptions in this study are based on the TESLA approach and thus all references to the Linear Collider imply a 'cold' technology machine following the TESLA design.

To do precision physics, the e^+e^- collider must be a high energy, high luminosity machine. The TESLA design [2] is based on a 33 km long linac, that will be able to deliver energies of 0.5 to 0.8 TeV with possible extensions to 1 TeV or more, and a luminosity of $\mathcal{L} \approx 3.4 \times 10^{34}\, cm^{-2}\, s^{-1}$ for the 0.5 TeV machine.

1.2 The Top Quark

The top quark is nature's heaviest fundamental particle ever discovered. Because of this fact however, it is also the less precisely measured particle. A precise measurement of the top quark parameters is on its own right an important task for particle physicists, but furthermore, the value of its mass provides constraints on other searches of fundamental particles, such as the Higgs particle.

Fits of the SM parameters from the Electroweak working group at CERN provide constraints on the likely mass of the Higgs particle that is currently the big unsettled question of the SM. The left plot of figure 1.1 shows the likely mass of the Higgs particle depending on our knowledge of the mass of the W and the mass of the top quark.

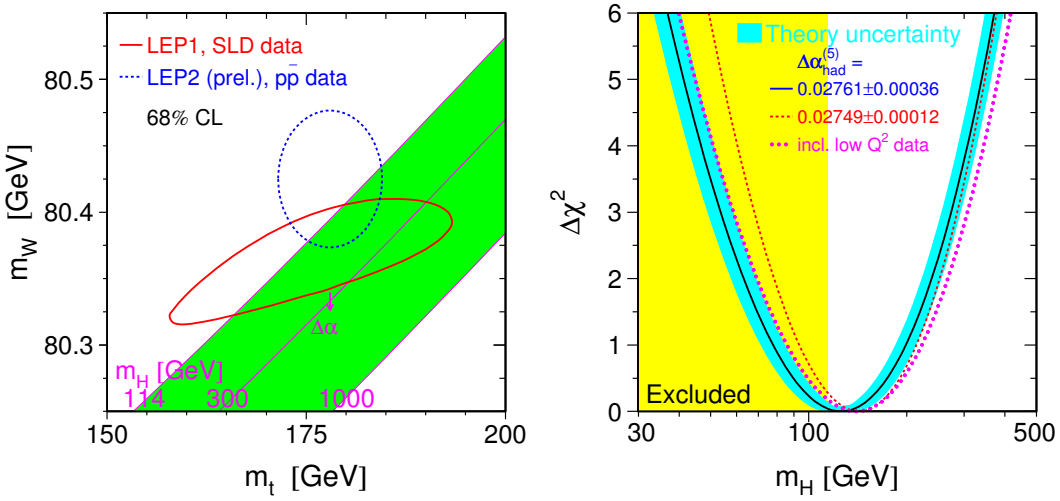

Figure 1.1: *Left*: The dependence of the masses of the W and the top quark to the mass of the Higgs boson. *Right*: The blue band plot for Winter 2005 [3]

It is clear from this plot that a smaller uncertainty of the mass of the top quark would help in constraining the mass of the Higgs more precisely in the 68% CL. On the right in figure 1.1 is the famous 'Blue Band' plot showing the χ^2 fit of all the SM parameters versus the mass of the Higgs, and this plot is also sensitive to the mass of the top quark.

The top quark in an e^+e^- machine is produced in pairs via the channel of figure 1.2. This means that in order for top quarks to be produced, the machine must operate at the top quark production threshold energy of $2M_t \approx 350$ GeV. Furthermore, in the TESLA design linear collider the production rate for $t\bar{t}$ is $70\,h^{-1}$ for the 0.5 TeV machine [2].

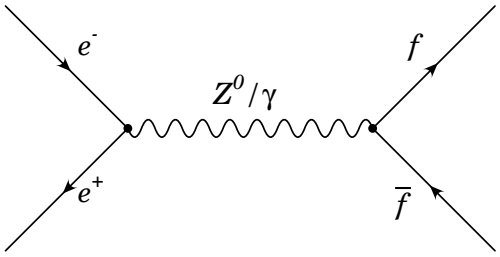

Figure 1.2: The main channel for top quark production in e^+e^- collisions, the fermion states on the right are in our case a $t\bar{t}$ pair.

The attempt for top quark physics at an e^+e^- machine has both advantages and disadvantages, the main advantage is that for the channel shown in figure 1.2, the $t\bar{t}$ pair mainly decays to $t\bar{t} \to b\bar{b}WW$ which have clear signatures. Also, since the top is so heavy, it decays very rapidly so that high order QCD corrections are cut-off. The main disadvantage, which comes also from the fact that the top is heavy, is that because of its large mass and hence fast decay, the 'toponium' $t\bar{t}$ pair fails before even a complete oscillation, and thus no clear toponium resonance exists in the cross section.

In this analysis, standard values for the top quark parameters had to be assumed, and since according to the Particle Data Group the current limits on the top mass are $M_t = 174.3 \pm 5.1$ GeV for direct observation and $M_t = 178.1^{+10.4}_{-8.3}$ GeV from electroweak fits [1], a central value of $M_t = 175$ GeV is assumed in the analysis. Furthermore, the width of the top is assumed to be $\Gamma_t = 1.43$ GeV and the strong coupling constant is taken at the Z^0 peak as $\alpha_s(M_Z) = 0.118$, so as to be consistent with the assumption for M_t.

1.3 Machine Energy

Every particle physics accelerator is characterized by its energy. For a LC of 0.5 TeV, the electron and positron beams are both expected to have an energy of 250 GeV at the interaction point, thus creating a centre of mass energy of 0.5 TeV. However, this will be a 33 km long machine, so the actual energy delivered at the interaction point might be very different from the nominal energy that the operators have set the machine to

run at. Furthermore, within each accelerated bunch of particles, physics and machine effects can cause the bunch to have a non-uniform energy, thus also influencing the actual energy of the collisions at the interaction point.

Therefore, a way of describing and monitoring the actual machine energy must be devised. The luminosity spectrum of an accelerator is such a way of describing the beam energy for the incoming particles of each collision.

The luminosity is usually described as:

$$\mathcal{L} = flux \times N \quad [cm^{-2}s^{-1}]$$

and the luminosity spectrum is then:

$$\frac{\partial \mathcal{L}}{\partial \sqrt{s}}$$

where N is the number of particles in the beam, and $\sqrt{s}$ is the centre of mass energy.

Most of the physics analysis of the events produced by the collision of the two beams depends on the knowledge of the centre of mass energy of each collision, which itself depends on the luminosity spectrum of the machine. Hence, the luminosity spectrum is a very important parameter in the physics studies of an accelerator, and must be understood, modeled and measured very carefully and precisely.

2 Luminosity Spectrum

2.1 Energy Losses

The beam energy of an accelerator usually has physics and machine related effects influencing its value. The way to describe it is to understand and measure precisely the luminosity spectrum of the machine.

In the ILC, there are three main energy losses influencing the luminosity of the machine. These are:

Initial State Radiation (or ISR) is the physics process in which the electrons (positrons) in the accelerating beams emit a photon while they travel. The emitted photon carries some of the electron's momentum and thus the energy of the beam is reduced. ISR is calculable to high precision in QED, and thus can be modeled precisely.

BeamSpread (or BS) is the spread of energy introduced by the machine in each accelerated bunch of particles. Since the particles are accelerated in bunches, not all of them travel the same mean path, so depending on the position of each particle in the bunch, slightly different accelerating gradients are experienced, thus introducing a spread in the energy of the bunch[1].

BeamStrahlung (or BSTR) is a new energy loss mechanism, which is a result of the high energy and high luminosity of the machine. To achieve high luminosity, the beam size must be 'squeezed' as much as possible, and thus a strong electromagnetic field surrounds each bunch of accelerated particles. When the opposing bunches approach, each bunch 'feels' the opposing bunches' electromagnetic field, which exerts a transverse force on the bunches' particles, causing some of them to radiate photons, and thus lose energy. This effect increases in occurrence as the particle travels a greater path in the opposing bunch until it collides. Beamstrahlung is the most difficult of these three effects to model.

In figure 2.1, the three components of the luminosity spectrum can be seen plotted together. The x axis represents $\frac{\sqrt{s}}{\sqrt{s_n}}$, which is the ratio of the actual luminosity spectrum to the nominal.

The energy losses are included in the expression for the centre of mass energy of the machine such that:

$$\sqrt{s} = 2\sqrt{x_e x_p E_e E_p}$$

where the subscripts e and p stand for the electron and positron beams respectively, and,

$$x = x_{isr}\, x_{bstr}\, x_{bs}$$

are the contributions from each of the three loss mechanisms. A detailed derivation of this expression can be found in appendix A.

[1] Beamspread is not necessarily a loss mechanism, since because of it, some particles in a bunch might end up with higher than the nominal beam energy

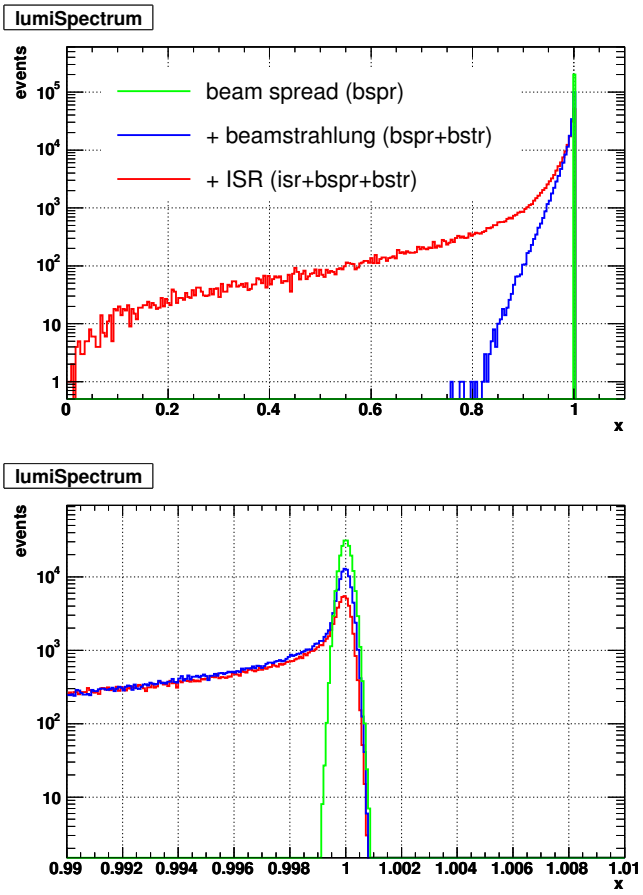

Figure 2.1: The three components of the luminosity spectrum

2.2 Modeling the Components

In order for the luminosity spectrum to be as accurate as possible, a detailed understanding of each of its three components must exist.

ISR is calculable to high precision in QED, and in our analysis it is calculated using the PANDORA Monte Carlo generator [4]. Beam spread is expected to be of a Gaussian shape, and with a spread of 0.1% for the electron beam and 0.03% for the positron beam [2]. The most difficult of the components to model is beamstrahlung.

There are two ways in which beamstrahlung can be modeled, either parametrized into a function, or modeled at the microscopic level for each particle in the bunch. The standard way of parameterizing beamstrahlung is by using the Circe function [5]. The Circe function is

$$f(x) = a_0 \cdot \delta(1-x) + a_n x^{a_2}(1-x)^{a_3} \tag{2.1}$$

with a_0, a_2 and a_3 the parameters and a_n a normalization factor. The δ function

represents the particles that have not radiated, while the β function represents the particles that have radiated.

The second way of modeling beamstrahlung is by modeling the microscopic interactions of the collisions. The program Guinea-Pig [6] provides the framework for modeling the microscopic interactions of bunch-bunch collisions. In figure 2.2, a sample histogram of the beamstrahlung and beamspread components of the luminosity spectrum can be seen.

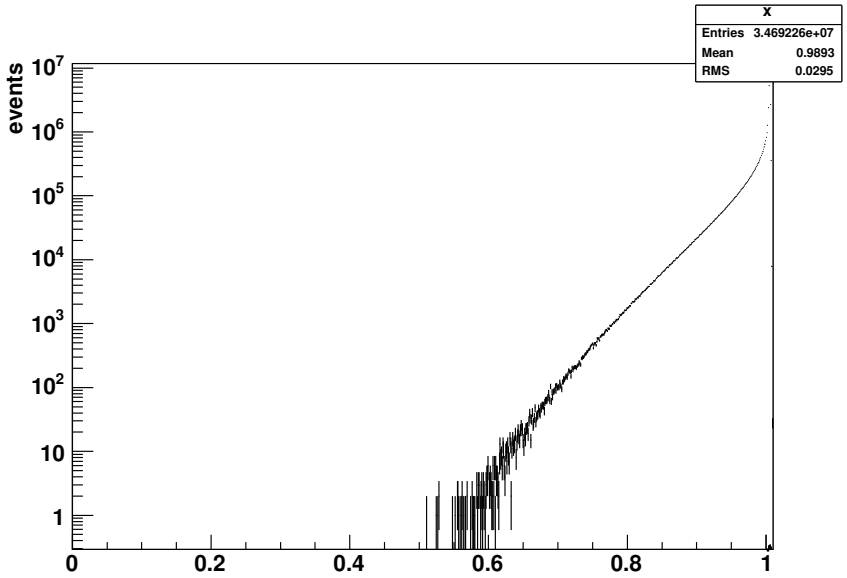

Figure 2.2: Luminosity spectrum including beamstrahlung and beamspread, based on the microscopic simulation of 550 bunch-bunch collisions.

This specific data set is the simulation of 550 bunch-bunch collisions simulated with Guinea-Pig, including full accelerator effects simulated by the program FONT (Feedback On Nanosecond Timescale) [7].

The problems that arise in these two approaches are that, when the Circe function is called to fit a realistic luminosity spectrum, problems are introduced because the function is divergent at 1, and realistic luminosity spectra with beamspread go to higher values than 1. The Guinea Pig microscopic simulation approach is a useful way for obtaining data sets but cannot be used to parametrize existing luminosity spectra.

Thus, a more flexible and efficient way is needed in order to be able to parametrize the beamstrahlung and beamspread components of the luminosity spectrum. Such that the parameters for the beamstrahlung and the spread can be read from a fit of the function to the full (BSTR + BS) luminosity spectrum.

2.3 Parameterizing Beamstrahlung and Beamspread

The Circe function provides an insufficient way of modeling realistic luminosity spectra, because such spectra also include beamspread effects, and such effects cause the spectrum to go to higher values than $\frac{\sqrt{s}}{\sqrt{s_n}} = 1$, but the Circe function, because of its β function component, diverges at one, and thus does not provide a complete parametrization of the spectrum.

In order to obtain a function that would provide a parametrization for both the tail of plot in figure 2.2, corresponding to beamstrahlung, and the Gaussian peak centered around 1, corresponding to beamspread, the most trivial approach would be to convolute the two functions describing these parts of the spectrum.

$$\int Circe \otimes Gaussian \, dx$$

However, this integral is impossible to be done analytically, since this would correspond to doing an integral of the β function $a_n x^{a_2}(1-x)^{a_3}$ in the region (0, 1), and since the β function diverges at 1, this is impossible.

Thus, there is a need for an alternative function to be constructed, which would provide a description of the luminosity spectrum in its complete range. The criteria for this new function are positivity and integrability in the $(0, 1)$ range [5].

Furthermore, it must be noted that the search for such a function is difficult, since as it can be seen in figure 2.2, the spectrum rises very fast in the (0.8, 1) region, such that it increases by approximately 4 orders of magnitude, also in the (0.6, $\sim$ 0.85) region, a slight curvature can be observed, which increases the complication for selecting an appropriate parametrization form.

2.4 New Parametrization

After exploring various different possibilities of functions that could be used for describing the luminosity spectrum, and satisfying the criteria for integrability and positivity, the following form was decided to be the basis for the new parametrization,

$$f(y) = a_0 \frac{e^{-y^2/2\sigma^2}}{\sqrt{2\pi}\sigma} + \frac{1}{\sqrt{2\pi}\sigma} \int_0^1 (\sum_{i=1}^{n} a_i n(b_i z) e^{-b_i z}) \times e^{-(y-z)^2/2\sigma^2} dz \qquad (2.2)$$

where y is the mapping $y = 1 - x$, a_0 and a_i are fractional weights, and the $n(b_i z)$ are the normalizations of the exponentials.

The description of the components of function 2.2 is as follows: the first component represents a unit normalized Gaussian, centered around $y = 1 - x$, with the a_0 factor being the weight of the term. The next part of the function consists of the integral of a sum of exponentials, convoluted with a Gaussian. The integral is definite and runs from 0 to 1, since this is the 'region of (physical) interest' of the function, describing the luminosity spectrum. Also a way is needed to 'kill' the function outside this 'region of interest', and this way is accommodated by the integration running from 0 to 1. Furthermore, the a_i are the weights of the terms in the sum (convoluted exponential(s)

with Gaussian), the $n(b_i z)$ terms are the normalizations for each of the exponentials, the σ represents the spread of the Gaussians, and the z is the 'dummy' index of integration for the convolution. The details of the definitions and the integration can be found in appendix B.

The 'physical' meaning of the terms is that the 'stand-alone' Gaussian resembles the behavior of the δ function in equation 2.1, but with a spread σ which corresponds to the beamspread effect, and the sum of exponentials convoluted with a Gaussian are terms that should describe the different sloped regions of the luminosity spectrum. The Gaussians are both unit normalized, and the $n(b_i z)$ factors are included to unit normalize the exponentials[2], such that the whole function is unit-normalized and the fractional weights have a meaning. Through the fractional weights then, when this function is fitted to a realistic luminosity spectrum, the different contributions of the spectrum can be 'read out', as it will be demonstrated in the following section.

The sum of the exponentials to be convoluted (n) is left open to run over an undefined number of terms, since this is a free parameter that can be optimized according to the precision needed by the function.

2.5 Fitting `Real` Data

Now that we have a proposed form of a function describing the luminosity spectrum (beamstrahlung + beamspread), it is left to demonstrate that this function can indeed be used to parametrize a realistic luminosity spectrum, and that the parameters extracted from such parametrization are useful. The applicability and appropriateness of the proposed function can then be tested by the quality of the fit.

Such a data set is the one shown in figure 2.2, which is a simulated form of the luminosity spectrum as described in section 2.2, and includes most effects that can be simulated, both accelerator and physics related.

In order to do a fit with function 2.2 to the data, the number of exponential terms to be used must be decided. After investigations of various configurations, it was decided that the best fit to the data is provided when using $n = 4$ convoluted exponentials, as it will be explained below.

In order to comply with the unit normalization of the function, the data set was also unit normalized. In addition, an extra dx correcting factor was included in the Gaussian so as to get the form:

$$e^{-((y+dx)-z)^2/2\sigma^2}$$

This was done in order to correct for the possibility that the luminosity spectrum data set does not peak exactly at 1, but has a shifted peak. So, with this extra term, possible offsets can be 'read' from the fit, and determine the exact position of the peak. In the case that the spectrum does peak exactly at 1, then the dx factor returns as zero.

[2]It can easily be proved that the convolution of two unit normalized functions yields a unit normalized result.

The fit of the function[3] to the Guinea-Pig data can be seen in figure 2.3, with the fitted parameters and the different regions of the fit zoomed for more accurate illustration.

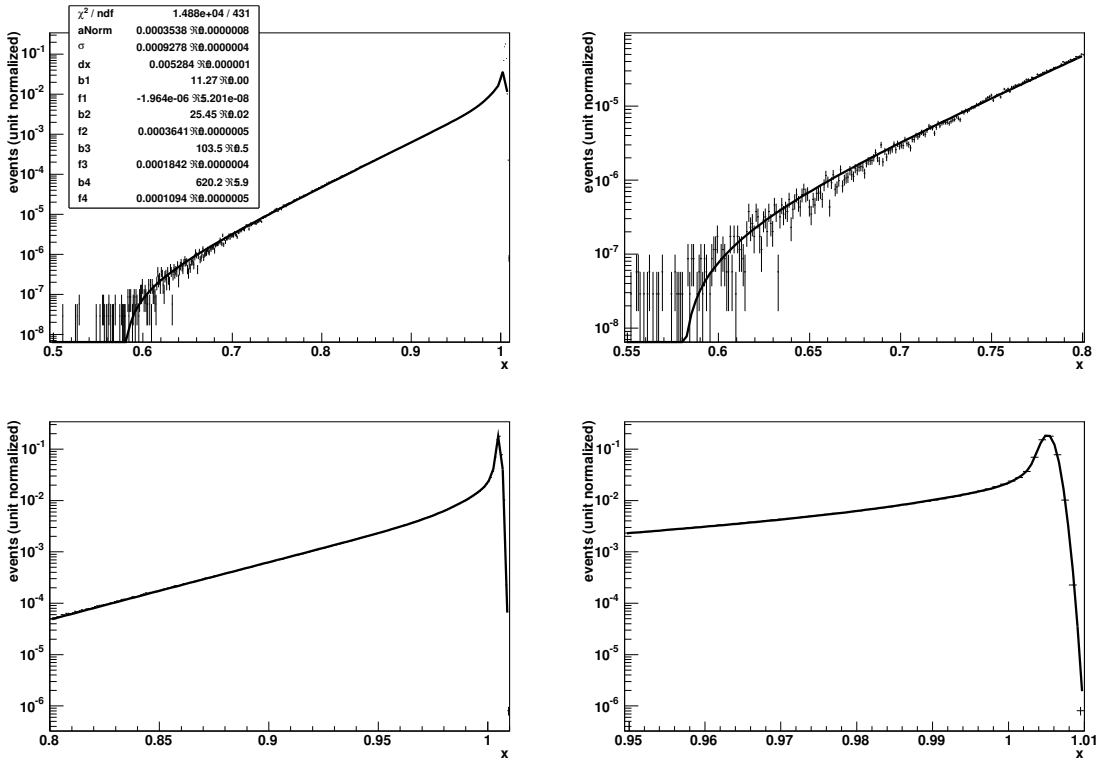

Figure 2.3: Clockwise from top left: Luminosity spectrum fitted with new parametrization; zoomed in different regions of the fit.

It can be seen in the plots above that the function does indeed provide a good fit to the data, eventhough the χ^2 fit does return to about ~ 30 per degree of freedom, but it can be argued that this is due to a computational problem having to do with the histogram itself, and not the quality of the fit.

Furthermore, the fractional weights returned from the fit need to be corrected by dividing them by 10^{-3}, since they correspond to a value per bin, so they need to be divided by the bin width in order to normalize them to correspond to a value per point. When this is done, it can then be checked that $(a_0 + a_1 + a_2 + a_3 + a_4) \approx 1$, which is what would be expected for fractions that conserve the unit area of the function, and thus this proves that the normalizations are correct.

The other parameters of the fit, namely the spread σ and the slopes of the exponentials, can also be interpreted. The spread, which would correspond to the beamspread

[3]Using MINUIT.

of the beam if assumed Gaussian, returned to be $\sigma = 0.093\%$, which is a good estimate of the original value of 0.1% used for the electron beam. Also, the correcting factor dx returned with a value of $dx = 0.0053$ which corresponds to an offset of the peak to 1.0053 instead of 1. In this case this is the result of statistical fluctations due to the method of simulating the dataset with Guinea-Pig, but in a real dataset this could indicate the effects of a complicated form of beamspread, which could shift the peak of the luminosity spectrum.

Finally, the 4 slopes of the exponentials returned as $b_1 \approx 11.3$, $b_2 \approx 25.5$, $b_3 \approx 103.5$ and $b_4 \approx 620.2$, which indicates which exponential is effective in which region of the spectrum. For example, in this case, the highest sloped exponential, namely b_4, takes care of the fit very near to the peak, where the one with the lowest slope, b_1, takes care of the tail of the data.

This can be further explained by examining the fractions returned. We can expect that the peak should have a large fraction of the function contributing to it, and it can be seen that the fraction of the stand-alone Gaussian is ~ 0.35, while if we include the fraction of the highest sloped exponential, the total contribution of the peak reaches ~ 0.46, meaning that it contains a large fraction of the function, as expected.

In addition, in order for the curvature at the tail of the data (0.55-0.6 region) to be described by the function, the fraction of the lowest sloped exponential, b_1,(i.e. the exponential that contributes in that region) turns negative, as to kill the function by providing the curvature of the tail. This however, introduces some complication in our fit, which will be described below.

A way to better understand the fit of the function to the histogram containing the Guinea-Pig generated luminosity spectrum can be provided by examining the residual plots, i.e. the value of $\frac{H_i - f(x_i)}{H_i}$, the fractional difference of the histogram value to the function value evaluated for each bin of the histogram.

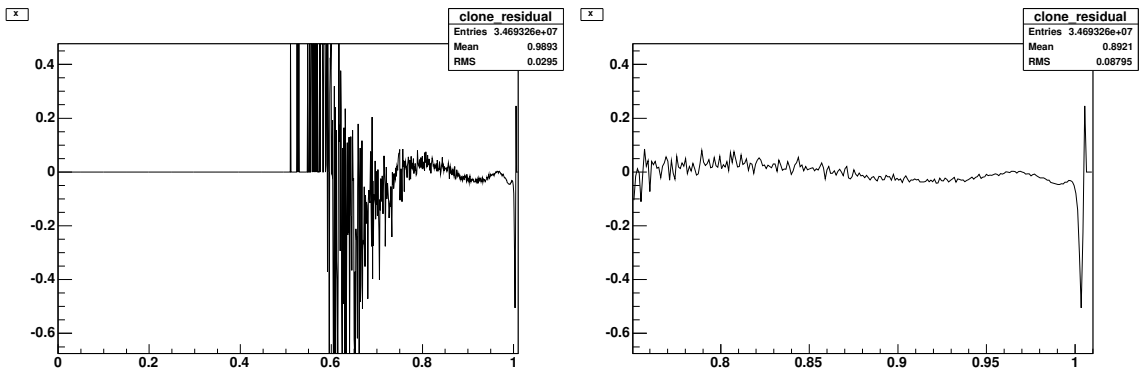

Figure 2.4: Residual plots of the fractional difference of the histogram value to the function value evaluated at each bin.

By examining the residual plots of figure 2.4, we can observe that there is a significant difference of the value of the histogram to the function in the region (0.5, 0.65),

i.e. the region of the lowest sloped exponential.

This difference is due to the fact that the curvature of the data at that region is very difficult to fit with exponentials, thus introducing large differences when examined in the form of residual plots. Also, the function decays rapidly in that region to provide the curvature required, but it never drops exactly to zero, thus this creates a large effect in the residual plots for the case that the histogram bin value is zero, and the function value is not. Furthermore, there seems to be a disagreement between function value and data value at 1 (the peak), but in fact this is a property of the fit, since we are fitting a function to a histogram, at the peak the function cannot fit perfectly all the bins, so in this case, it underestimates the bin containing the peak, and overestimates the previous one, in order to correct for this effect. However, this is an artifact of fitting such steep spectra to a function, and should not be considered as a problem.

In addition, the end tail (0.5 - 0.7 region) of the luminosity spectrum contains 5-6 orders of magnitude less data than the peak, and thus should be considered as a region of low statistics that does not have an important contribution to the overall effect of the spectrum. Nevertheless, it is desirable to have a very precise description of it.

There are further issues that can be discussed in the context of choosing the form of equation 2.2, namely the number of exponentials used to fit the function and the form of the lowest sloped exponential that is effective in the 0.5 - 0.7 region of the spectrum.

This fit was also attempted with 2 and 3 exponentials, and it was found that then the tail of the spectrum is neglected by the function, with the fit forcing the 3 (or 2) exponentials used to concentrate on a high slope, thus looking after the mid and peak ranges of the spectrum. Therefore, depending on the range of the spectrum that is of interest, the function can be adjusted in order to accommodate this, by decreasing the number of exponentials used. It was also attempted to use 5 exponentials, but then the function turns degenerate, with the extra exponentials canceling each-other, and thus the quality of the fit decreases. Therefore, in the context of describing the full range of the spectrum, the optimum number of exponential terms to be used was found to be $n = 4$ in equation 2.2.

Furthermore, in order for the fit to describe the low slope tail region of the spectrum, alternative ways of forming the killing term were examined. By artificially adding a term of the form:

$$\frac{1}{\sqrt{2\pi}} \int_0^1 (1 - z^\lambda)(a_i n(b_i z) e^{-b_i z}) \times e^{-(y-z)^2/2\sigma^2} dz$$

as the 4^{th} exponential, where λ is a free parameter of the fit, the 'killing' of the function describing the tail of the spectrum becomes more accurate, and the χ^2 of the fit decreases. However, this artificial inclusion of the 'killing' term $(1 - z^\lambda)$ spoils the normalization of the function, and the fractional weights that were used to describe the contribution of the different components of the fit of the function to the spectrum lose their significance.

Also, this then introduces terms such as

$$\sim \int_0^1 z^\lambda e^{-b_i z} dz = \Gamma(\lambda, b)$$

into the integration, where $\Gamma(\lambda, b)$ is a Gamma function, and this brings further complication into the proposed function.

Finally, it is proved that the function of the form described in 2.2 provides an accurate and flexible description of the the beamstrahlung and beamspread components of the luminosity spectrum, and the parameters in the parametrization provide a useful way of describing features of the spectrum and 'reading' from it properties such as the beamspread (if assumed Gaussian).

2.6 Numerical Convolution

A different approach for obtaining a parametrization of the luminosity spectrum that would include beamspread was also attempted. This different approach corresponds to performing a numerical convolution of the Circe function 2.1 with a Gaussian. If the algorithm for the numerical convolution is carefully constructed, then the problems that arise in the analytic integration approach of the divergence of the β function in Circe, can be overcome.

Two different methods were used for the numerical convolution of Circe with a Gaussian, one doing the convolution using a Monte Carlo (MC) random number method, and a very preliminary attempt for doing a trapezium integration of the two functions in question.

In the MC algorithm, a distribution was used describing a β function and multiplied by a Gaussian random number distribution describing the beamspread. For the δ function, a random number Gaussian distribution centered about 1 was also used. For each event in the MC algorithm, the selection of which part of the Circe $\otimes$ Gaussian function would the event correspond to (i.e. the δ function part of Circe or the β function part), was made by examining the coefficients of the two parts of Circe (equation 2.1), and using a uniform random number distribution to make the choice.

The histogram version of the convoluted functions with the standard parameters for Circe (table 1) can be seen in figure 2.5.

a_0	0.5461
a_2	20.297
a_3	-0.62747

Table 1: Standard Circe parameters as used in [8]

It can be seen in the plots of figure 2.5 that the convolution results in the shape that would be expected for the the luminosity spectrum describing beamstrahlung and beamspread.

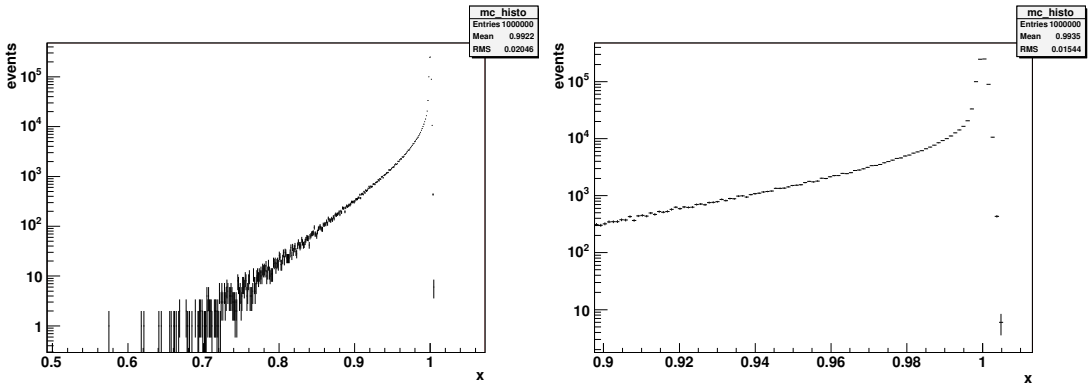

Figure 2.5: MC convoluted Circe with a Gaussian, using the standard parameters for Circe (table 1), and a Gaussian spread of 0.01%.

The algorithm used to produce this spectrum does depend on the Circe parameters, and the spread of the Gaussian, and thus could be used as a function in order to fit the realistic luminosity spectrum and extract the parameters of Circe and beamspread from it. However, the 'know-how' of doing such a fit could not be obtained in the limited time available for this project, and thus this is left as a future task to be done to test the correctness and usefulness of the numerical convolution.

In addition to the MC numerical method, a very preliminary attempt to do the same convolution using a standard trapezium rule method was attempted. However, this proved to be more difficult that anticipated, since the Circe function has the distinct feature of rising so fast to 1, and thus for the trapezium rule to be used, extra care must be taken in order to obtain an adequate sampling of the function in the sensitive fast rising region. Thus, methods of adaptive integration are needed in order for such an approach to work, and again the limited time of this study did not allow for such methods to be developed.

2.7 Fitting `Fake` Data

The development of the methods described in section 2.6 allows a further test on the parametrization developed in section 2.4 to be performed.

Assuming that the MC convolution is accurate, a simple form of a luminosity spectrum depending on Circe and including beamspread can be obtained, and thus the proposed new parametrization can be tested by fitting the function to the histogram containing the MC convoluted spectrum.

The plot of the fitted spectrum, together with a zoomed version concentrating on the peak (the most difficult and important part to fit) can be found in figure 2.6.

By examining the parameters returned by the fit, it can be seen that the χ^2 in this case returns a negligible value, indicating that the fit is good, in addition the value of the beamspread extracted from the fit is $\sigma = 0.098\%$ which is in good agreement with

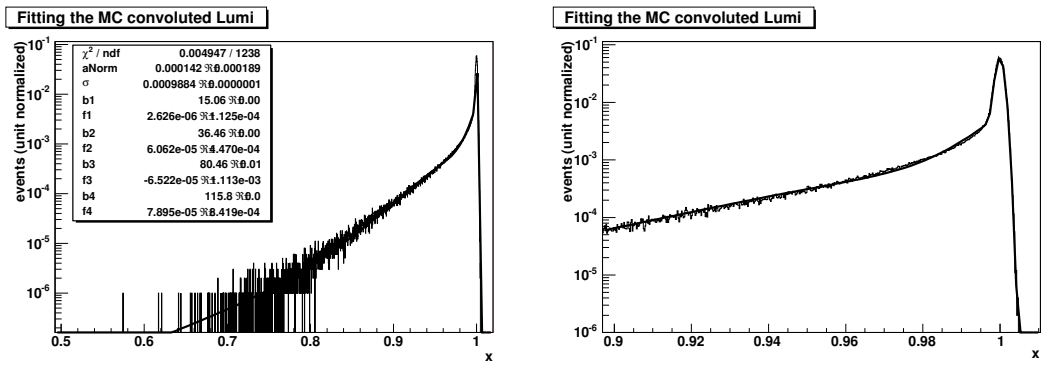

Figure 2.6: Fit of the new parametrization to a histogram containing data from the MC convolution of Circe with a Gaussian.

the value of $\sigma = 0.1\%$ that was used for the convolution. Furthermore, the slopes b_i are as expected, and the fractional weights need again to be corrected to correspond to values per point instead of values per bin, thus dividing with the bin width of the histogram.

Due to the simplicity of the spectrum fitted (compared with the more realistic spectrum of section 2.5), the function has turned degenerate, with exponentials 2 and 3 having roughly equal and opposite fractions. This indicates that the fit could be also be performed with a version of function 2.2 containing $n = 3$ exponentials.

This proves again that the parameterization described in section 2.4 gives a flexible and accurate way of parameterizing spectra with beamstrahlung and beamspread effects.

3 Top Quark Threshold Studies

At the ILC, top quarks are mainly produced via the channel of figure 1.2, with a $t\bar{t}$ pair produced in the final state. The ILC cross-section for such a process is [5]:

$$\frac{d\sigma^{e^+e^-}}{d\Omega}(\sqrt{s}) = \int_0^1 dx_1 dx_2 D_{e^+e^-}(x_1, x2, \sqrt{s}) \frac{d\sigma_0^{e^+e^-}}{d\Omega'}(x_1, x_2, \sqrt{s}) \tag{3.1}$$

where in the integral the $D_{e^+e^-}$ is the energy spectrum, and $\frac{d\sigma_0^{e^+e^-}}{d\Omega'}$ is the bare cross-section. Thus, this suggests that the form of the energy spectrum has an important effect on the bare top cross-section.

This further implies that the uncertainty of the measurement of the top cross-section heavily depends on the knowledge of the luminosity spectrum of the machine, because if the luminosity spectrum is inaccurate, then a systematic error is introduced in the extraction of the top quark parameters. In fact, it is believed that this is the factor introducing possibly the largest error on the top quark parameters in such a measurement at the ILC.

The objective of this simulation is to examine the effects of the luminosity spectrum to the parameters of the top quark, as they would be measured in an e^+e^- linear collider.

3.1 Technology Used: Cross-Sections

In order to calculate the bare cross-section of equation 3.1, the program TOPPIK [9] was used, which provides a NNLO calculation of the the cross-section near the threshold. The results from this calculation were then interpolated in order to provide the cross-section as a function of centre of mass energy of the collisions. This resulted in cross-sections of the form of figure 3.1

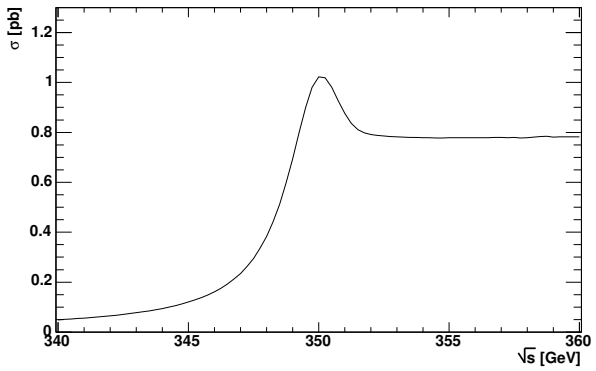

Figure 3.1: The cross-section as calculated by TOPPIK for a 175 GeV top quark.

For the task of being able to interpolate between different cross-section top quark parameters, the cross-sections were stored in such a way as to contain different versions of the same calculation, but for different top quark parameters, thus resulting in different cross-sections. An example of the cross-sections contained of a file can be seen in figure 3.2.

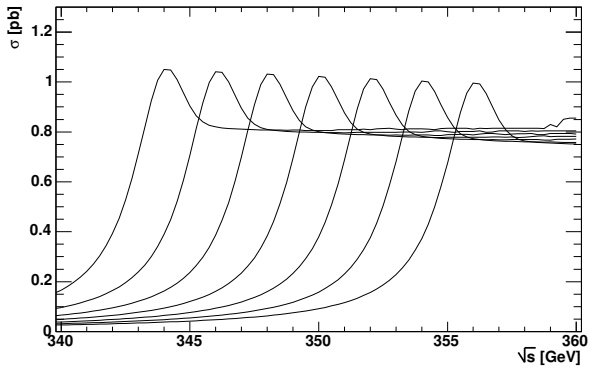

Figure 3.2: A sample file containing cross-sections for different values of the top quark mass.

This allowed the analysis to be done in way such that the files storing information about the cross-section to behave as 4 dimensional functions of the form $f(M_t, \Gamma_t, \alpha_s; \sqrt{s})$, and thus to be able to fit with them. The need for this fitting procedure will be apparent in the following sections.

The standard top quark parameters used, as mentioned in section 1, are:

M_t	175 GeV
Γ_t	1.43 GeV
$\alpha_s(M_Z)$	0.118

Table 2: Standard top quark parameters used in the analysis.

3.2 Effects of the Luminosity Spectrum

The luminosity spectrum heavily influences the cross-section for top quark production, as it is described in equation 3.1. Thus, by convoluting a function that describes the luminosity spectrum with the bare cross-section, we can obtain the cross-section that would be expected to be measured in the machine.

This convolution can be done for different spectra / different parameters of a spectrum, and by comparing the resulting cross-sections, we can determine the effect of this change in the luminosity spectrum to the top quark parameters.

In addition, we can perform this analysis by switching on and off the different energy losses described by the luminosity spectrum, as explained in section 2.1, and observe the response of the cross-section to these changes.

The plot of figure 3.3 illustrates this idea, by describing the bare cross-section, and then adding one by one the different energy losses, which lead to the smearing of the cross-section.

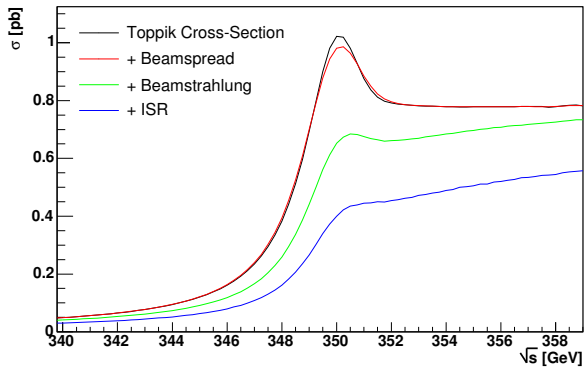

Figure 3.3: The effect of introducing the three main energy losses to the bare cross-section.

The smeared cross-section loses some of the bare cross-sections' characteristics, such as the peak, and thus in order to know what to expect from the ILC, a detailed understanding of the luminosity spectrum must exist. In addition, by examining the uncertainties of our knowledge of the luminosity spectrum, the uncertainties in the parameters of the top quark can be deduced, at it will be demonstrated in the following sections.

The basic idea behind this simulation is to produce a theoretical cross-section, smear it with a form of the luminosity spectrum, then smear the same cross-section with a slightly different luminosity spectrum, and by fitting the two cross-sections, obtain the differences that would be introduced to the top quark parameters by the variation of the spectrum.

3.3 Fitting Method

In order to fit the two smeared cross-sections, one must be treated as the data obtained from the actual experiment, and the other as the theoretical simulated cross-section.

Therefore, a way must be devised in order to allow us to create a "data" sample from a smeared cross-section.

Also, in the data cross-section, additional effects introduced by the experimental methods used to do such analysis will be introduced. These effects include assigning the number of points that the threshold scan of the accelerator would concentrate on

(i.e. in which energies would the accelerator run in order to obtain enough data to fully describe the top threshold cross-section), and the integrated luminosity per scan point, as well as the detector efficiency for collecting the data.

In the analysis, this is done by sampling a number of points from the theoretical cross-section, and multiplying them with the integrated luminosity to be used, and with a fractional number describing the detector efficiency.

In this analysis, unless otherwise stated, a choice of using 20 scan points equally distributed in the regions from 346 GeV to 354 GeV, with an integrated luminosity of $\int \mathcal{L} = 3 \times 10^4$ pb per point, and a detector efficiency of 41% [10], were used.

A sample plot of a "data" cross-section extracted from a simulated theoretical cross-section can be seen in figure 3.4 below:

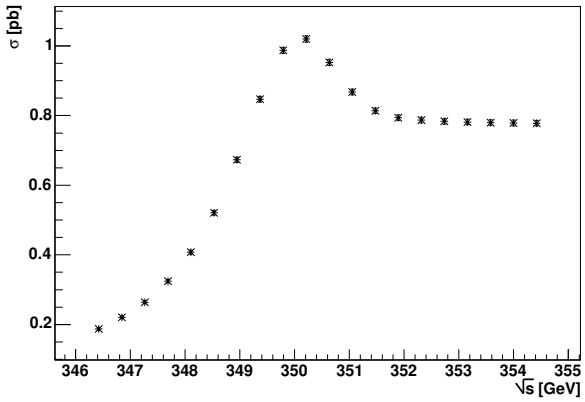

Figure 3.4: A sample of "fake data" as extracted from a theoretical cross-section.

The next step is to fit the theoretical cross-section to the data with different parameters for its luminosity spectrum. This is done using a χ^2 test for the top quark parameters, from MINUIT, and minimizing it using Migrad. From this fit, the change in the parameters due to the difference of the two cross-sections can be obtained, as well as the statistical uncertainty and various correlations of the fitted parameters.

The change of the parameters is then interpreted as the systematic shift due to the difference in the luminosity spectra used to smear the cross-sections, and this can be used in many ways to explain the effect that different forms of spectra would have on the top measurement, as well as the effect that uncertainties in our ability to know (measure) the spectrum precisely, would have on the top parameters.

The outcome of such a fit can be seen in figure 3.5, where the same smeared cross-section is used for both data and fit, in order to illustrate that the method works. The results on the fitted parameters indicate no shift from the input values, as would be expected for a fit of two identically smeared cross-sections.

Now that the framework for examining the effects of different luminosity spectra on the top quark parameters has been introduced, we can proceed by examining more

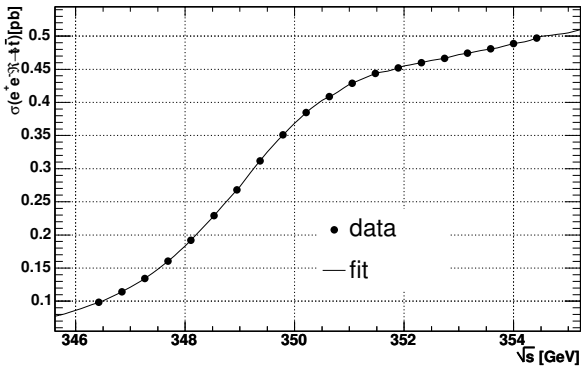

Figure 3.5: The plot of a 'sample' fit, illustrating that the method works.

realistic cases of such effects.

3.4 Varying Beamspread

The first component of the luminosity spectrum to be examined for the effects it introduces to the top quark parameters is beamspread.

When the decision was taken for the ILC to follow the 'cold' TESLA technology, one of the factors influencing it was that with a 'warm' technology, the luminosity spectrum was expected to be more complicated, by including a complicated form of beamspread with a 0.3% spread. In this analysis we simplify the situation by assuming that the beamspread would have 0.3% spread, but with a simple Gaussian shape.

We want to examine how the comparison of two luminosity spectra with different beamspread contributions, one with the predicted 'cold' technology 0.1% spread, and one with a 0.3% spread, influences the top parameters. Another way to interpret this is that we expect the beamspread of the machine to have a 0.1% spread, but in reality it has a 0.3% spread, thus introducing a difference in the results.

The bare cross-section smeared with a standard ISR calculated through PANDORA, and a Circe function with the standard parameters described in section 2.6, but with a Gaussian beamspread of 0.3%, is to be considered as the 'data' cross-section. The cross-section that is fitting the data (i.e. the expected theoretical cross-section), is the bare cross-section smeared with the same effects, but a beamspread of 0.1%.

The fit of the theoretical cross-section to the data can be seen on the left in figure 3.6, and the χ^2 of the fit as a function of M_t can be seen on the right. The minimum of the χ^2 indicates the value of M_t that better fits the data.

From the plot on the left, it can be seen that the peak in the data cross-section which is smeared with a higher value for beamspread, has slightly shifted to a lower $\sqrt{s}$ value in comparison to the theoretical cross-section used for the fitting. The relative shift in the top parameters introduced by the difference of beamspread in the two

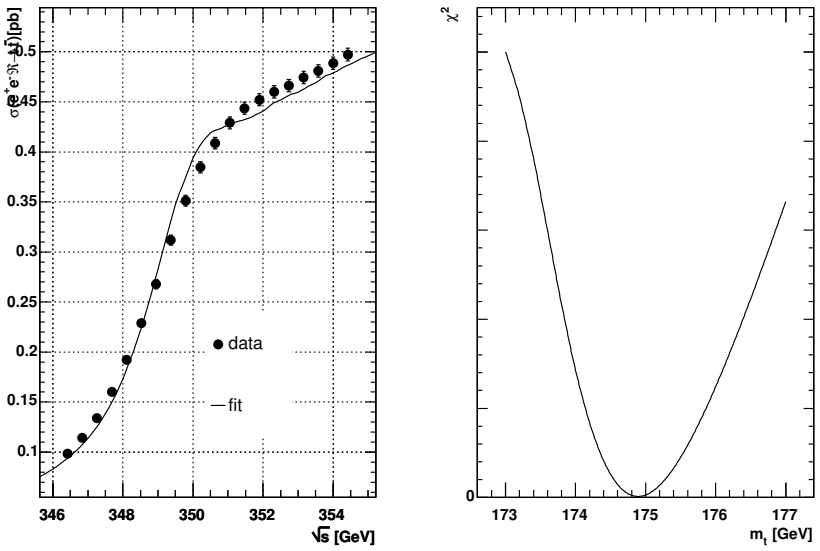

Figure 3.6: *Left*: Fitting theoretical cross-section to the data, the data having a 0.3% beamspread, and the theoretical cross-section a 0.1%. *Right:* The χ^2 of the fit as a function of M_t.

cross-sections can be found on table 3. From the values of the shifted parameters it can be seen that the effect of a higher beamspread is rather large on the top mass, as it shifts it by -118 ± 12 MeV. Thus, this implies that the beamspread of the machine must be monitored precisely, in order to avoid the systematic errors introduced by an uncertainty in it.

Parameters	Systematic Shift	Statistical Error
δM_t	-118 MeV	$\pm$12 MeV
$\delta\Gamma_t$	30 MeV (at limit)	$\pm$4 MeV
$\delta\alpha_s(M_Z)$	-0.0028	$\pm 3.3 \times 10^{-4}$

Table 3: Shift in the top parameters introduced by a variation of the beamspread of the Luminosity Spectrum.

The shift in Γ_t must not be considered obsolete, since the parameter has reached its fitting limit, and thus the true shift could be larger than the one stated here. However, this gives an indication that a large shift is introduced in its value.

These results indicate that beamspread has a large effect on the parameters of the top quark, and thus that an accurate knowledge of it is needed for the ILC, in order to be able to do a precision measurement of the top quark mass. This further

indicates however, the need for having a parametrization of the luminosity spectrum that includes beamspread, as it was argued in section 2.4.

3.5 Varying Beamstrahlung

The next component of the luminosity spectrum that needs to be investigated for its effects to the top parameters is beamstrahlung.

In this analysis, the traditional form of beamstrahlung parametrized using Circe is used, with the standard parameters of section 2.6 for the smearing of the fitting function. For the smearing of the 'data' points to be fitted, varied Circe parameters are used, and by the fits, the effects of the variations can be studied.

In order to decide by what amount the Circe parameters are to be varied, two approaches were used. The first approach follows the estimated errors obtained for the Circe parameters by simulating the measurement of the luminosity spectrum using the acolinearity of Bhabha events in the forward-tracking region at TESLA [11]. In this paper, a form of the Circe parameters is chosen, such that a luminosity spectrum can be constructed. By simulating the process of measuring this luminosity spectrum using the acolinearity of Bhabha events [12] in the forward-tracking region of TESLA, the uncertainties on the Circe parameters arising from the measurement are estimated. Thus, by using these uncertainties, we can estimate the variation of the top parameters introduced by them.

The uncertainties estimated in [11] are based on a slightly different version of the Circe parameters than the one used in this analysis, thus they must be adjusted to our Circe parameters. The resulting parameters with uncertainties are:

a_0	0.5461	$\pm 4.97 \times 10^{-3}$
a_2	20.297	± 0.2045
a_3	-0.62747	$\pm 6.06 \times 10^{-3}$

Table 4: Standard Circe parameters with uncertainties adjusted from [11].

By adjusting the Circe parameters with different permutations of the uncertainties from table 4, and creating the data set from them, the effect introduced to the top parameters can be studied. This can be interpreted as supposing that the true luminosity spectrum intrinsic to the machine is the one with the Circe parameters having the standard form, but the measurement of the luminosity spectrum using the Bhabha acolinearity method can only deliver the Circe parameters with the precision described in table 4. Thus, the effect of having a luminosity spectrum measurement efficiency as described in [11] to the top quark measurement can be studied.

It must be noted, that for the luminosity spectrum described both in [11] and in this analysis, the standard TESLA beamspread of 0.1% is included.

The plots of figure 3.7 are the outcome of the fitting for the Circe parameters of $a_0 = 0.5461 + 4.97 \times 10^{-3}$, $a_2 = 20.297 + 0.2045$ and $a_3 = -0.62747 + 6.06 \times 10^{-3}$, i.e. the standard Circe parameters with the upper error bound applied to them. The

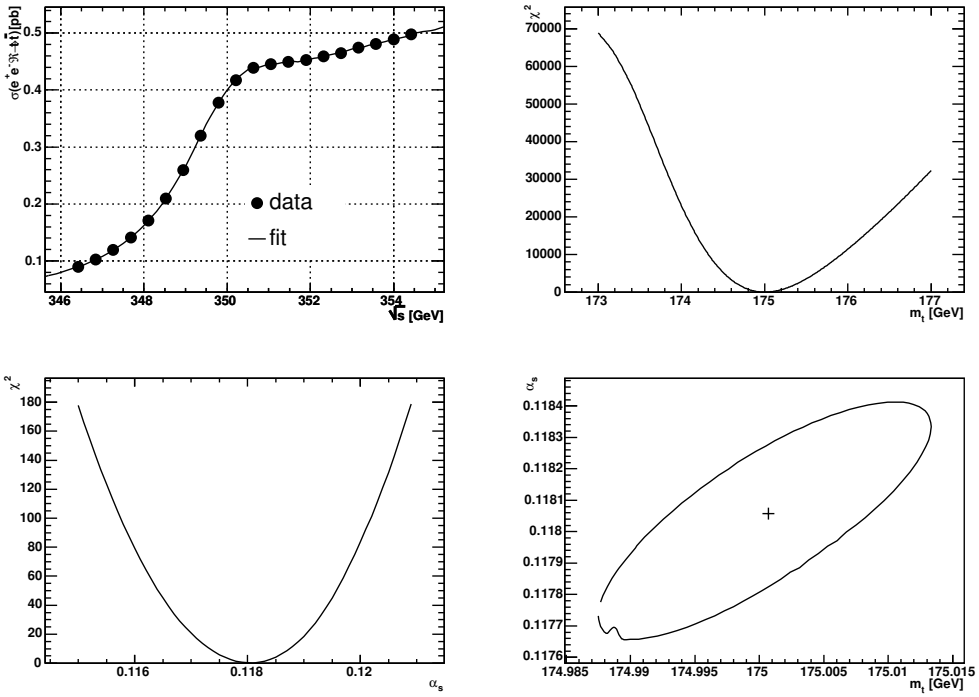

Figure 3.7: Clockwise from top left: The fit of the theoretical smeared cross-section to the data cross-section; the χ^2 of the fit as a function of M_t; the contour plot in the $M_t - \alpha_s$ parameter space, indicating the correlation of the two parameters; and the χ^2 of the fit as a function of α_s.

plots, clockwise from top left, describe the fitting of the theoretical standard Circe smeared cross-section to the Circe + errors smeared data cross-section, the χ^2 of the fit as a function of M_t, the contour plot in the $M_t - \alpha_s$ parameter space, indicating the correlation of the two parameters, and χ^2 of fit for the α_s parameter.

The systematic shifts resulting from the errors due to acolinearity method (for all upper bound errors), as can be seen in table 5, are negligible and well within the statistical errors introduced by the fit. In addition, the results of the other permutations of combining the Circe errors are similar, with the statistical error always being greater than the small (if any) systematic shift observed.

This result implies that the Bhabha acolinearity is a valid method to be used for measuring the luminosity spectrum at the top quark threshold, since the small uncertainties that are introduced do not affect the top parameters. However, these errors do not include uncertainties introduced to the luminosity spectrum (and hence the Circe parameters) due to the accuracy of the forward region detector that would be used to measure the acolinearity. Such uncertainties can introduce a significant effect to the top parameters.

Parameters	Systematic Shift	Statistical Error
δM_t	1 MeV	$\pm$13 MeV
$\delta\Gamma_t$	-0.14 MeV	$\pm$10 MeV
$\delta\alpha_s(M_Z)$	6×10^{-5}	$\pm 3.8 \times 10^{-4}$

Table 5: Shift in the top parameters introduced by a variation of the Circe parameters to accord with the uncertainty introduced by the luminosity spectrum measurement using the Bhabha acolinearity method.

Since the beamstrahlung parameterization uncertainties due to the Bhabha acolinearity method do not significantly affect the top parameters, larger uncertainties to the Circe parameters must be introduced in order to investigate how the luminosity spectrum and the top parameters respond to a significant change in the beamstrahlung parameterization.

The uncertainties to be studies were randomly chosen to be $\pm 5\%$ and $\pm 10\%$ of the standard Circe parameters.

The effect of luminosity spectrum with all Circe parameters in the $\pm 5\%$ and $\pm 10\%$ bounds to the top cross-section compared to the cross-section smeared with the standard Circe parameters can be seen in figure 3.8.

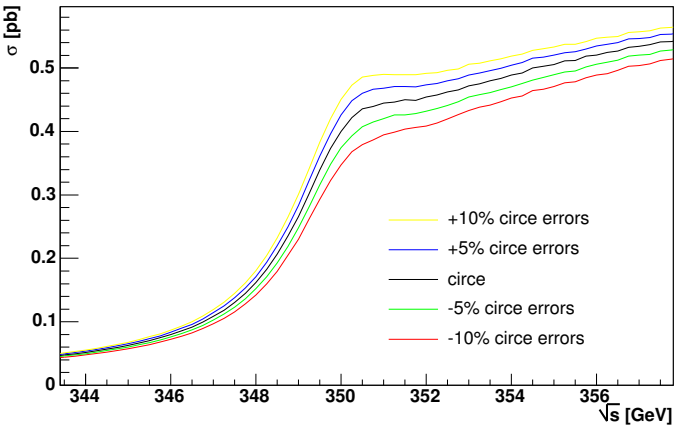

Figure 3.8: Effect of $\pm 5\%$ and $\pm 10\%$ errors for Circe in the top cross-section.

It can be seen from figure 3.8 that such uncertainties in the Circe parameters symmetrically shift the position of the cross-section in the $\sqrt{s}$ axis.

In figures 3.9 and 3.10, the fits of the standard Circe luminosity spectrum cross-section to data with standard Circe parameters $+5\%$ and $+10\%$ respectivelly, can be seen. The plots of the fits of the cross-sections with Circe -5% and -10% luminosity spectra are symmetrically identical.

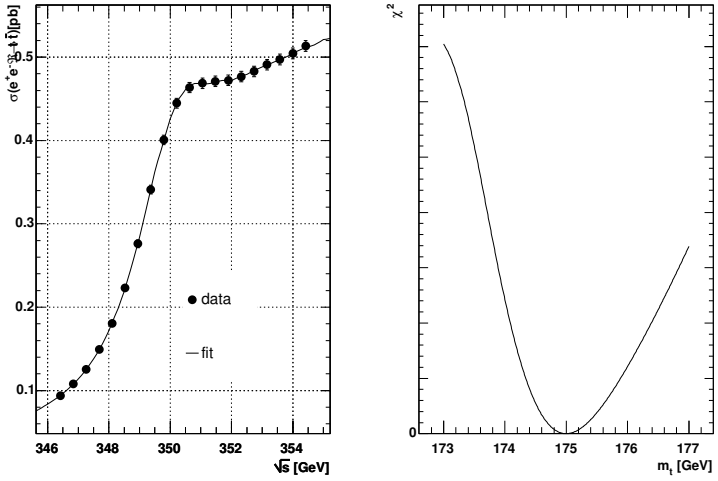

Figure 3.9: Fit of the standard Circe luminosity spectrum convoluted cross-section to the Circe + 5% as data.

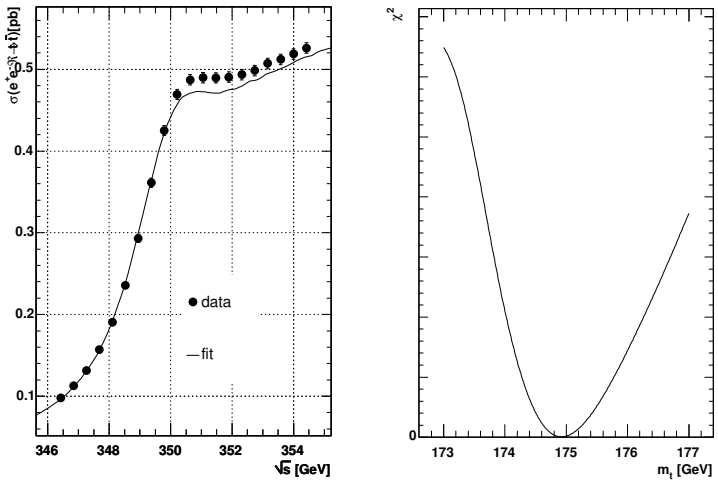

Figure 3.10: Fit of the standard Circe luminosity spectrum convoluted cross-section to the Circe + 10% as data.

The results of the fitting for the top parameters are summarized in table 6. As it can be seen from these results, the main point to be made is that the top parameters (especially M_t) seem to be more sensitive to the -5% and -10% versions of Circe,

Circe	Parameters	Systematic Shift	Statistical Error
+10%	δM_t	-76 MeV	$\pm$7.1 MeV
	$\delta\Gamma_t$	at limit	–
	$\delta\alpha_s(M_Z)$	at limit	–
+5%	δM_t	-3 MeV	$\pm$7.6 MeV
	$\delta\Gamma_t$	+3 MeV	$\pm$9.4 MeV
	$\delta\alpha_s(M_Z)$	+ 0.003	$\pm 4.9 \times 10^{-3}$
−5%	δM_t	+14 MeV	$\pm$8.2 MeV
	$\delta\Gamma_t$	+4 MeV	$\pm$8.8 MeV
	$\delta\alpha_s(M_Z)$	at limit	–
−10%	δM_t	+121 MeV	$\pm$7.9 MeV
	$\delta\Gamma_t$	at limit	–
	$\delta\alpha_s(M_Z)$	at limit	–

Table 6: Shift in the top parameters introduced by a variation of the Circe parameters by $\pm$5% and $\pm$10%.

since the systematic shift for these is significantly larger than the respective +5% and +10% versions. For example, the −10% Circe version gives a shift $\delta M_t = +121 \pm 7.9$ MeV, while the respective positive version of the Circe errors, namely +10%, gives a shift of $\delta M_t = -76 \pm 7.1$ MeV. In addition, the −5% Circe version gives a systematic shift in M_t larger than the statistical error, while the +5% version has a shift within the statistical error, and also the α_s parameter for the −5% version of the fit reaches its limit, while the value for +5% version does not, thus it changes slower, since the limits are identically set at 0.115 - 0.121.

This result does imply that the fits for the Circe parameters behave worse for more heavily smeared cross-sections, since as it can be seen from figure 3.8, the −5% and −10% Circe smeared cross-sections are relativelly more smeared than the rest, thus beamstrahlung is a larger effect for these cross-sections, and so information used for the fitting are smeared out, which causes the fitted parameters to have this asymetrical behaviour.

3.6 Effective Luminosity Spectrum for Top Production

This part of the study concentrates on investigating how does the luminosity spectrum influences top quark production. The luminosity spectrum describes the differential luminosity of the machine, and is a function of $\frac{\sqrt{s}}{\sqrt{s_n}}$ where $\sqrt{s}$ is the effective centre of mass energy, and $\sqrt{s_n}$ is the nominal. However, at the top threshold, the luminosity spectrum should contribute to top production only near $\frac{\sqrt{s}}{\sqrt{s_n}} = 1$, since below this value, the threshold for top production is not reached, so no top events exist.

This investigation can be made by truncating the luminosity spectrum to different percentages about the peak, and applying this to the top analysis described in the previous sections. In more detail, the truncated luminosity spectrum can then be applied to the cross-section and treated as the data, while a full spectrum applied to the cross-section is to be treated as the fitting theoretical cross-section.

Samples of truncated luminosity spectra can be seen in figure 3.11.

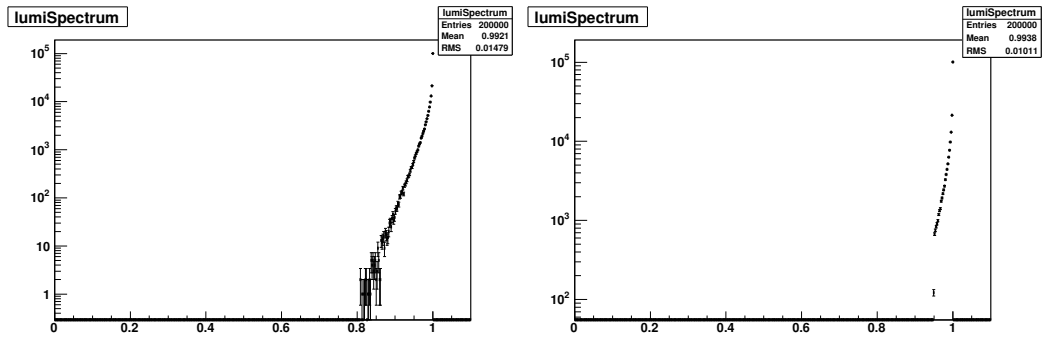

Figure 3.11: *Left:* 80% truncated Luminosity spectrum *Right:* and 95% truncated spectrum.

By applying luminosity spectra with different truncated values, the effectiveness of the luminosity spectrum on the top threshold can be determined. The effectiveness of the luminosity spectrum is the percentage that contributes to top production, and thus the percentage on which we need to have an accurate knowledge and description in order for the top measurement to be as precise as possible.

The results for δM_t of the fits of the standard beamstrahlung + beamspread (Circe + Gaussian) luminosity spectrum to different truncated luminosity spectra can be seen in figure 3.12.

It can be seen in this plot that the effect of truncating the luminosity spectrum up to 97%, i.e. using only 3% of its value around the peak to the top cross-section, does not influence the top parameters. The systematic shift, and thus the truncation affecting the top parameters, starts by truncating 98% and on.

In figure 3.13, the effect of the truncation of the luminosity spectrum to the Γ_t and α_s parameters are shown. In the left plot, the effect of truncating the luminosity spectrum on $\delta\alpha_s$ can be seen, with the same truncation percentage as the turning point

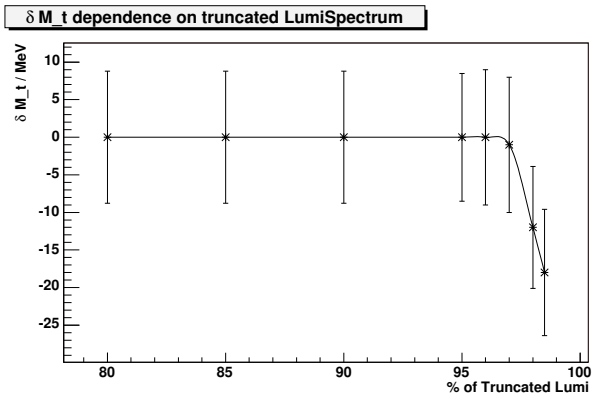

Figure 3.12: The effect of truncated luminosity spectra on δM_t.

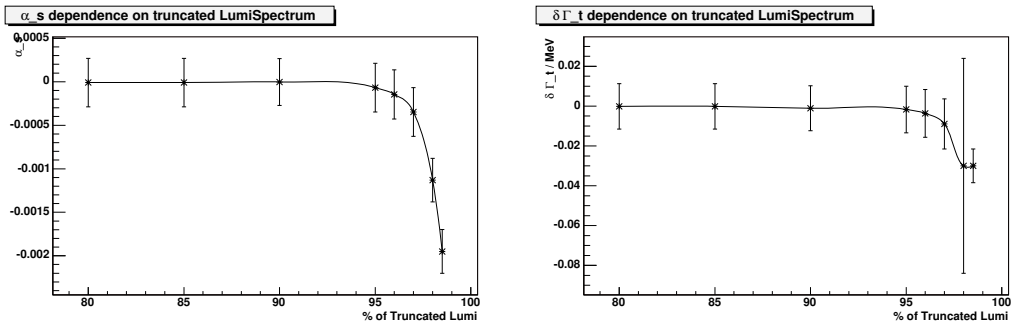

Figure 3.13: *Left:* Effect of truncated luminosity spectra on $\delta\alpha_s$ *Right:* and $\delta\Gamma_t$
NOTE: In the Γ_t plot, the fit reaches its limit beyond 98% of the truncated spectrum.

where the systematic effects are introduced. In the plot on the right, the effect of the truncation on $\delta\Gamma_t$ is shown, in this plot it must be noted that the fit reaches its limit beyond 98% of the truncation. However, the tendancy for the value of α_s to shift can be observed from the previous points, as well as the large amount that α_s shifts by.

These results indicate that if there is a very accurate knowledge of the peak of the luminosity spectrum ($4-5\%$ of the spectrum around the peak) at the top threshold, then that is adequate for the analysis of the top parameters to be unaffected by errors in the knowledge of the tail of the spectrum.

However, in a more realistic context, the spectrum around the peak will always have a small uncertainty associated with it (from the measurement), and thus the description of the 20% of the spectrum around the peak must be known, in order to help and understand the uncertainties at the peak.

3.7 Need for a Scan Strategy

In the top threshold analysis of this study, essentially a random number of points was used in order to determine how the experimental data would be distributed, and thus deduce the change in the top parameters from fits to these data points. However, for a more realistic and accurate analysis to be done, an optimization of the scan strategy to be followed when the ILC runs at the top quark production threshold must be determined.

In a real machine run, an amount of integrated luminosity ($\sim$ running time or data obtained) at the top threshold will be issued, and with that amount of data the experimenters must proceed by making the most accurate measurement possible for the top parameters.

This measurement however, depends on how the threshold scan is planned, since the fit to the data is affected by the way the points and the integrated luminosity per point are distributed.

Therefore, a detailed study of how it is best for the top threshold to be scanned must be made. This includes determining which region in the centre of mass energy is important for mapping the top cross-section, and thus which should be the starting and ending $\sqrt{s}$ of the top threshold scan. The next issue to be answered is how to distribute the given integrated luminosity in that region, with how many points and what integrated luminosity per point to be used.

By examining these questions, an equilibrium must exist between the answers that would provide the most accurate description of the top cross-section, which would optimize the fit to work on the best configuration of data, and thus keep a high level of accuracy for this aspect of the top threshold analysis.

The analysis presented in this report would then be optimized to resemble the realistic analysis that will take place when the ILC runs at the top threshold.

A very preliminary attempt was made for the scan strategy analysis, but due to the limited time of the project, this essentially consists of asking the questions that need to be answered. More effort in this part of the top quark threshold analysis is required, in order for the simulations of the threshold studies to become more realistic.

4 Conclusions and the Future

This study has provided some very interesting results about the luminosity spectrum and studies of the top quark threshold at the ILC.

The need for a more flexible parameterization of the beamstrahlung energy loss of the luminosity spectrum, such as to incorporate beamspread, was identified. Such a parameterization was constructed, and was successfully tested against simple and complicated luminosity spectrum data sets. Furthermore, a method was devised for creating a beamstrahlung + beamspread parameterization by numerically convoluting Circe with a Gaussian, but this approach needs further effort in order to demonstrate its applicability.

The top quark threshold analysis was performed by investigating how the top quark cross-section responds to variations of the luminosity spectrum. This study was performed for luminosity spectra with different beamspread, indicating that the top quark parameters are very sensitive to the variation of beamspread. Also, by using different parameterizations for Circe and hence different beamstrahlung contributions to the luminosity spectrum, the effects to the top parameters were examined.

These differences in the parameterization of beamstrahlung included changing the parameters by the amount indicated in [11], that would be the uncertainty introduced by using the Bhabha acolinearity to measure the luminosity. This resulted in negligible systematic changes to the top quark parameters, and hence we can conclude that the top quark measurements are not sensitive to the uncertainties introduced by using this method for measuring the luminosity spectrum.

In addition, a random variation of $\pm 5\%$ and $\pm 10\%$ on the beamstrahlung parameters was investigated, and it was demonstrated that the top parameterers are sensitive to such large variations of the beamstrahlung parameters, and in particular this sensitivity is asymetric in the sense that the -5% and -10% versions of the parameterization give a larger shift than the $+5\%$ and $+10\%$. This arises because the smaller Circe parameters indicate a stronger beamstrahlung effect, as it can be seen in figure 3.8, and thus the top cross-section is more heavily smeared, causing it to lose some of its characteristics and thus influencing the fit to the standard cross-section.

Finally, the percentage of the luminosity spectrum that is effective for top quark production was investigated, and it was demonstrated that only 3% about the peak of the spectrum is important for top production. However this does not necessarily imply that the rest of the spectrum is not important, since in order to have an accurate knowledge of the peak, which is a difficult region to measure, knowledge of how the luminosity spectrum behaves is needed.

Future improvements of this study include the optimization of the scan range for the top quark threshold, in order to adjust the simulation of the top measurement accordingly. In addition, a wider range in the parameter space of the fits should be chosen, such that the fitted parameters do not reach the fit limit so rapidly.

On the parameterization front, the effect of the difference of the function to the data set, as illustrated in the residual plots of figure 2.4, must be further examined, such that the function is best optimized in all regions. Also, a larger sample of differ-

ent spectra can be fitted with the function, in order to explore in full the functions' flexibility.

The numerical convolution approach should be further developed as well, such that the convolution algorithm can be used as a function that can fit data, and through this fitting to examine the usefulness of the parameters extracted from the fits.

Finally, it is worth noting that the top threshold study is a model depended approach, that does not provide the absolute errors on the top measurements at the ILC [13]. Nevertheless, it is a very interesting study to indicate the effects of our understanding of the luminosity spectrum to the measurement of the top quark, and also to impose estimated limits on the precision that can be reached in such measurement.

Acknowledgments

I would like to thank Prof. David Miller for his continued support during these last three years, and for providing an inspiring and stimulating supervision during the twists and turns of this study. Also I feel indept to Dr. Stewart Boogert for providing the framework for this study to be made, for the many helpful discussions about project related (and unrelated) topics, but most of all for giving me the opportunity to work on such an interesting and exciting project.

Finally, I would like to thank Dr. Mark Lancaster for always being willingly available for consultation, and always at a very short notice.

A Centre of Mass Energy Derivation

In a linear collider, the electron (e) and positron (p) beams travel in opposite directions. Thus they can be described by the energy-momentum four vectors:

$$p_e = (x_{isr}x_{bs}x_{bstr}E_e, 0, 0, x_{isr}x_{bs}x_{bstr}\mathbf{E}_e)$$

and

$$p_p = (x_{isr}x_{bs}x_{bstr}E_p, 0, 0, -x_{isr}x_{bs}x_{bstr}\mathbf{E}_p)$$

by making the decision that the electron beam travels in the positive x direction, and thus the positron beam travels in the negative x. In this expression, x_{isr} is the energy loss due to ISR, and is in the range $0 \leq x_{isr} \leq 1$, x_{bstr} is the energy loss due to beamstrahlung and is in the range $0 \leq x_{bstr} \leq 1$, and x_{bs} is the energy loss due to beamspread, and in principle can have any value, we can assume however that $-\frac{\sigma}{2} \leq x_{bs} \leq \frac{\sigma}{2}$, where σ is the value of beamspread.

Now by using the convention that $x_e = x_{isr}x_{bstr}x_{bs}$ are the energy loses of the electron beam, and $x_p = x_{isr}x_{bstr}x_{bs}$ those of the positron beam, we can write:

$$\mid p_e + p_p \mid = (x_eE_e + x_pE_p, 0, 0, x_e\mathbf{E}_e + x_p\mathbf{E}_p)$$

$$\Rightarrow x_e^2E_e^2 + 2x_ex_pE_eE_p + x_p^2E_p^2 - (x_e\mathbf{E}_e + x_p\mathbf{E}_p)^2 = s$$

$$\Rightarrow x_e^2E_e^2 + 2x_ex_pE_eE_p + x_p^2E_p^2 - x_e^2E_e^2 - 2x_ex_p\mathbf{E}_e \cdot \mathbf{E}_p - x_p^2E_p^2 = s$$

and by canceling the identical terms,

$$\Rightarrow 2x_ex_p(E_eE_p - \mathbf{E}_e \cdot \mathbf{E}_p) = 2x_ex_p(2E_eE_p) = 4x_ex_pE_eE_p = s$$

Taking the square root of both sides then leads to the expression,

$$\sqrt{s} = 2\sqrt{x_ex_pE_eE_p}$$

where $\sqrt{s}$ is the standard form of expressing the Lorentz invariant centre of mass energy of a collision.

B Details of the new Parameterization

We want to construct a function that has a behavior such as figure 2.2 with exponentials.

The first step is to map the exponentials to rise from $x = 0$ to $x = 1$ by defining:

$$y = 1 - x$$

Then the function of choice to be used is:

$$f(y) = a_0 \frac{e^{-y^2/2\sigma^2}}{\sqrt{2\pi}\sigma} + \frac{1}{\sqrt{2\pi}\sigma} \int_0^1 (\sum_{i=1}^{n} a_i n(b_i z) e^{-b_i z}) \times e^{-(y-z)^2/2\sigma^2} dz \tag{B.1}$$

where a_0 is the fractional weight of the 'stand-alone' unit normalized Gaussian, and the a_i's are the fractional weights of the convoluted exponentials.

The $n(b_i z)$ are the normalizations of the exponentials such that:

$$n_i = \frac{1}{\int_0^1 e^{-b_i z}} = \frac{b_i}{1 - e^{-b_i}}$$

So by having a normalized Gaussian convoluted with normalized exponentials, the result of the convolution is normalized as well.

Now, if the integration in B.1 is carried out analytically, the final result is:

$$f(y) = a_0 \frac{e^{-y^2/2\sigma^2}}{\sqrt{2\pi}\sigma} + \frac{1}{2}\{\sum_{i=1}^{n} e^{\frac{1}{2}b_i(b_i\sigma^2 - 2y)} a_i n_i (-Erf[\frac{b_i\sigma^2 - y}{\sqrt{2}\sigma}] + Erf[\frac{1 + b_i\sigma^2 - y}{\sqrt{2}\sigma}])\} \tag{B.2}$$

where $Erf[z]$ is the Error function, the integral of a Gaussian distribution, and is defined as:

$$Erf[z] = \frac{2}{\sqrt{\pi}} \int_0^{\pi} e^{-t^2} dt$$

The function described in B.2 with n = 4, is the proposed form of a parameterization for the beamstrahlung and beamspread energy loss components of the luminosity spectrum.

References

[1] Eidelman et al. (Particle Data Group), Phys. Lett. B, **592**,1 (2004).

[2] TESLA Technical Design Report, http://tesla-new.desy.de/

[3] LEP ElectroWeak Working Group, CERN, 2005. http://lepewwg.web.cern.ch/LEPEWWG/

[4] M. Peskin and M. Iwasaki, *Pandora, and Pandora-Pythia: Event Generation for Linear Collider Physics*. http://www.slac.stanford.edu/ mpeskin/LC/pandora.html

[5] T. Ohl, *CIRCE Version 1.0: Beam Spectra for Linear Collider Physics*, Comput.Phys.Commun. 101 (1997) 269-288. [hep-ph/9607454]

[6] D. Schulte, Ph.D. Thesis, University of Hamburg 1999; TESLA-97-08.

[7] The FONT project, http://hepwww.ph.qmul.ac.uk/ white/FONT/default.htm.

[8] S. Boogert, QCD and Top sessions, ECFA meeting, Durham, Sept. 2004.

[9] A.H. Hoang and T. Teubner et al, *Top-Antitop Pair Production close to Threshold: Synopsis of recent NNLO Results*. [hep-ph/0001286].

[10] G. Blair, A. Juste, M. Martinez, D. Schulte, and C. Shepherd-Themistocleous. In DESY-ECFA Conceptual Design Report, DESY, 1997.

[11] K. Mönig, *Measurement of the Differential Luminosity using Bhabha events in the Forward-Tracking region at TESLA.*, LC NOTE: PHSM-2000-60-TESLA.

[12] M.N. Frary and D.J.Miller, *Monitoring the Luminosity Spectrum*, DESY 92-123A.

[13] N. Brambila et. al. *Heavy Quarkonium Physics*, [hep-ph/0412158].